Room-temperature single phase multiferroic magnetoelectrics: Pb(Fe, M)x(Zr,Ti)(1−x)O3 [M = Ta, Nb]

Dilsom A. Sanchez, Nora Ortega, Ashok Kumar, G. Sreenivasulu, Ram S. Katiyar, J. F. Scott, Donald M. Evans, Miryam Arredondo-Arechavala, A. Schilling, J. M. Gregg

Angaben zur Veröffentlichung / Publication details:

Sanchez, Dilsom A., Nora Ortega, Ashok Kumar, G. Sreenivasulu, Ram S. Katiyar, J. F. Scott, Donald M. Evans, Miryam Arredondo-Arechavala, A. Schilling, and J. M. Gregg. 2013. "Room-temperature single phase multiferroic magnetoelectrics: Pb(Fe, M)x(Zr,Ti)(1−x)O3 [M = Ta, Nb]." *Journal of Applied Physics* 113 (7): 074105. https://doi.org/10.1063/1.4790317.

Room-temperature single phase multiferroic magnetoelectrics: $Pb(Fe, M)_x(Zr,Ti)_{(1-x)}O_3$ [M = Ta, Nb]

Cite as: J. Appl. Phys. **113**, 074105 (2013); https://doi.org/10.1063/1.4790317
Submitted: 14 December 2012 • Accepted: 27 December 2012 • Published Online: 20 February 2013

Dilsom A. Sanchez, Nora Ortega, Ashok Kumar, et al.

Room-temperature single phase multiferroic magnetoelectrics: $Pb(Fe, M)_x(Zr,Ti)_{(1-x)}O_3$ [M = Ta, Nb]

Dilsom A. Sanchez,[1] Nora Ortega,[1] Ashok Kumar,[2] G. Sreenivasulu,[3] Ram S. Katiyar,[1,a)] J. F. Scott,[4] Donald M. Evans,[5] Miryam Arredondo-Arechavala,[5] A. Schilling,[5] and J. M. Gregg[5]

[1]*Department of Physics, Institute Functional Nanomaterials, University of Puerto Rico, San Juan, Puerto Rico 00931-3343, USA*
[2]*National Physical Laboratory (CSIR), New Delhi 110012, India*
[3]*Physics Department, Oakland University, Rochester, Michigan 48309-4401, USA*
[4]*Cavendish Laboratory, Department of Physics, University of Cambridge, Cambridge CB3 0HE, United Kingdom*
[5]*Centre for Nanostructured Media, School of Mathematics and Physics, Queen's University, Belfast BT7 1NN, United Kingdom*

(Received 14 December 2012; accepted 27 December 2012; published online 20 February 2013)

We describe extensive studies on a family of perovskite oxides that are ferroelectric and ferromagnetic at ambient temperatures. The data include x-ray diffraction, Raman spectroscopy, measurements of ferroelectric and magnetic hysteresis, dielectric constants, Curie temperatures, electron microscopy (both scanning electron microscope and transmission electron microscopy (TEM)) studies, and both longitudinal and transverse magnetoelectric constants α_{33} and α_{31}. The study extends earlier work to lower Fe, Ta, and Nb concentrations at the B-site (from 15%–20% down to 5%). The magnetoelectric constants increase supralinearly with Fe concentrations, supporting the earlier conclusions of a key role for Fe spin clustering. The room-temperature orthorhombic C_{2v} point group symmetry inferred from earlier x-ray diffraction studies is confirmed via TEM, and the primitive unit cell size is found to be the basic perovskite Z = 1 structure of $BaTiO_3$, also the sequence of phase transitions with increasing temperature from rhombohedral to orthorhombic to tetragonal to cubic mimics barium titanate. © *2013 American Institute of Physics*. [http://dx.doi.org/10.1063/1.4790317]

I. INTRODUCTION

It has been known for several years[1–6] that the perovskite oxides $PbFe_{1/2}Ta_{1/2}O_3$ (PFT), $PbFe_{1/2}Nb_{1/2}O_3$ (PFN), and $PbFe_{2/3}W_{1/3}O_3$ (PFW) are multiferroics with long-range magnetic ordering near or above room temperature. Our earlier studies showed[7–17] that solid solutions of these materials with $PbZr_xTi_{1-x}O_3$ and pure $PbTiO_3$ yielded single-phase ferroelectric crystals whose weak ferromagnetism persists to room temperature or above. The low electrical conductivity of these materials thus produced a good alternative to $BiFeO_3$ for commercial device materials with intended embodiments as multiferroic memories,[18–21] sensors,[22] or voltage-controlled magnetic tunnel junctions[23–25] or THz generators.[26–28]

Of the members of this family of quaternary B-site perovskites, the Fe/W/Zr/Ti compounds exhibit only biquadratic coupling between polarization (P) and magnetization (M), and not linear magnetoelectricity. However, the remarkable dependence of electrically switched polarization P upon dc magnetic field H (vanishing above $H = 0.9$ T) due to magnetically dependent relaxation times[29] may still permit some practical devices. By comparison, the single-phase compounds with Fe/Ta/Zr/Ti or Fe/Nb/Zr/Ti at the B-site are linear magnetoelectrics at room temperature, with bilinear coupling in their free energy of form $G(P,M,T) = \alpha(T)_{ij}\, P_i\, M_j$. These materials are emphasized in the present report.

Semantics: since Fe spin clustering plays a key role in the room-temperature magnetoelectricity of these materials, it is useful to ask whether they may be considered to be nanocomposites rather than single-phase crystals. This is more a question of terminology than of physics, but usually composite designates a material with two or more well-defined substances, and a non-random distribution of B-site ions does not constitute two phases, nano-phases or otherwise. A few investigators[30] have asked whether these new materials are different from $BaTiO_3$ dilutely doped with Fe. Our answer is yes, because iron-doped barium titanate certainly has both magnetic and ferroelectric properties, but the magnetism is that of paramagnetic isolated impurities. If $BaTiO_3$ were heavily doped (several percent or more), it would be a new material and might have magnetoelectric properties; but it would be necessary to demonstrate that it is single-phase and that the Fe ions exhibit significant exchange coupling. We emphasize that single-phase materials need not have all ions perfectly ordered; there are many families of ferroelectrics that are disordered, some of which are relaxors.

II. EXPERIMENTAL

A. Sample preparation

Ceramic samples of $Pb(Fe_{0.5}Nb_{0.5})_x$ $(Zr_{0.53}Ti_{0.47})_{(1-x)}O_3$ (PFN_x-$PZT_{(1-x)}$) and $Pb(Fe_{0.5}Ta_{0.5})_y(Zr_{0.53}Ti_{0.47})_{(1-y)}O_3$ (PFT_y-$PZT_{(1-y)}$) were prepared by a conventional solid state reaction route. Analytical-purity oxides, PbO, ZrO_2, TiO_2,

a)Electronic mail: rkatiyar@hpcf.upr.edu.

Fe_2O_3, Ta_2O_5, and Nb_2O_5 (Alfa Aesar) with purity of 2-3 nines, were used as raw materials. The powders of the respective metal oxides were mixed in a planetary high-energy ball mill with tungsten carbide media and then were calcined at 850 °C for 10 h in a closed alumina crucible. 10% excess of PbO was added to each composition to compensate Pb deficiency during the high temperature processing. Poly (vinyl alcohol) solutions (1%) were added to the calcined powders as a binder. The dried powders were granulated by passing them through a 150 μm-mesh sieve and pressed using a hydrostatic press (3.5×10^8 Pa) into pellets of 10 mm diameter. The pressed pellets were heat treated at 600 °C for the removal of organic binders followed by sintering at 1100–1250 °C for 4 h. All heat treatments were performed in air. In order to prevent the PbO loss during high temperature sintering and to maintain desired stoichiometric, an equilibrium PbO vapor pressure was established with $PbZrO_3$ as setter by placing pellets in a covered alumina crucible. The flat polished surfaces of the sintered pellets were electroded with high purity silver paint and then dried at 200 °C before making electrical measurements.

B. Characterization techniques

Orientation and phase purity of the powders and sintered pellets were determined by x-ray diffraction (XRD) (Siemens D5000) using CuK_α radiation with wavelength of $\lambda = 1.5405$ Å. Raman measurements were performed in the backscattering geometry using the 514.5 nm line from an Ar laser. The scattered light was dispersed by T64000 spectrometer and collected with a charge-coupled device (CCD) detector. Ferroelectric hysteresis loops were measured at room temperature using a hysteresis loop tester (Radiant Technologies RT6000 HVS) at 50 Hz in a voltage range from 800 V to 1800 V. Magnetic measurements were carried out using a vibrating sample magnetometer (VSM). Dielectric measurements (capacitance and loss factor) were carried out in the temperature range of 100 to 700 °C for frequencies between 100 Hz and 1 MHz by using a programmable temperature controller (MMR K-20) and an impedance analyzer (HP 4294A). Field emission scanning electron microscope (FESEM; JEOL JSM-7500F) and a scanning transmission electron microscopy (STEM) equipped with energy-dispersive X-ray spectroscopy (EDX) was used to observe the chemical composition of the ceramic samples. The magnetoelectric voltage coefficient for ceramic samples of ~0.5 mm and poled in a constant electric field of 2.4 V/m (applied voltage = 1200 V) for 12 h was determined by dynamic methods as a function of bias field H at ac field $H_{ac} = 0.5$ Oe and frequency 1 kHz by measuring the voltage across the samples utilizing a lock-in-amplifier.

III. DISCUSSION

A. X-ray results: Structure and symmetry

Figure 1(a) shows the x-ray diffraction patterns for $Pb(Fe_{0.5}Nb_{0.5})_x(Zr_{0.53}Ti_{0.47})_{(1-x)}O_3$ (PFN_x-$PZT_{(1-x)}$) ($0.1 \leq x \leq 0.4$) ceramic samples. These results reveal single phase perovskite structure without the appearance of any secondary phase (e.g., pyrochlore). The diffraction patterns were

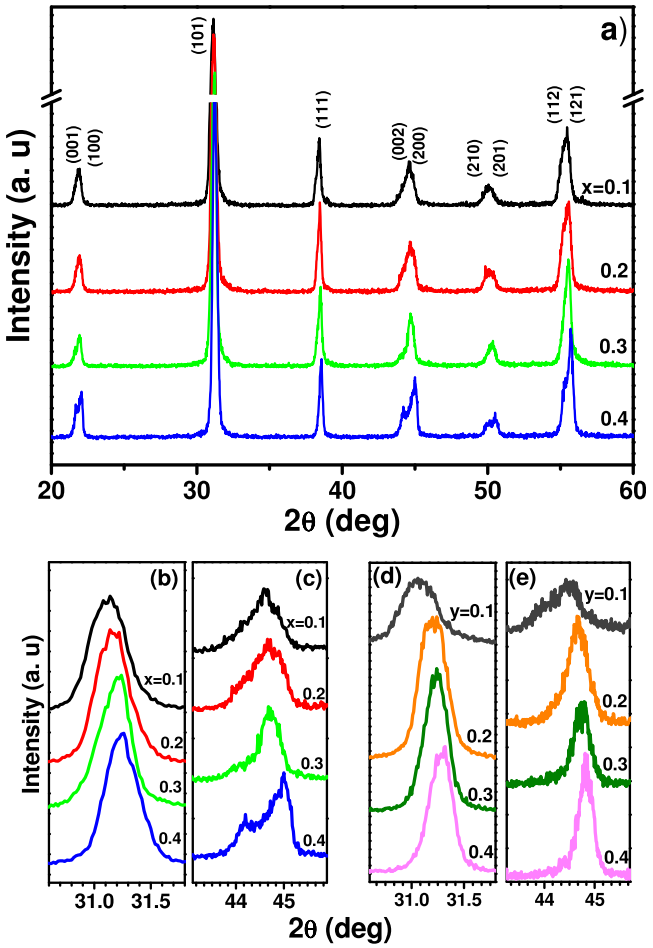

FIG. 1. Room temperature x-ray spectra of (a) $Pb(Fe_{0.5}Nb_{0.5})_x(Zr_{0.53}Ti_{0.47})_{(1-x)}O_3$ ceramics for different compositions ($0.1 \leq x \leq 0.4$). A close view of: (b) (101) and (c) (200) peaks for $Pb(Fe_{0.5}Nb_{0.5})_x(Zr_{0.53}Ti_{0.47})_{(1-x)}O_3$, (d) (101), and (e) (200) peaks for $Pb(Fe_{0.5}Ta_{0.5})_y(Zr_{0.53}Ti_{0.47})_{(1-y)}O_3$.

indexed, according to previously reported results for tetragonal $PbZr_{0.53}Ti_{0.47}O_3$ (PZT). This is an excellent result considering that the center of the perovskite octahedra could be occupied randomly by Nb^{5+}, Fe^{3+}, Zr^{+4}, or Ti^{+4}, which makes it difficult to obtain pure perovskite phase. Figures 1(b)–1(e) show a close view of the evolution of (101) and (200) peaks of (PFN_x-$PZT_{(1-x)}$) and (PFT_y-$PZT_{(1-y)}$) with x or y concentration, respectively. With the increase of PFN(x) or PFT(y) contents there is a systematic shift in the peak positions toward the higher diffraction angle (2θ) that could be due to substitution of ions with smaller ionic radii, in this case Zr^{4+} (0.72 Å) and Ti^{4+} (0.605 Å) by Ta^{5+}, Nb^{5+} (0.64 Å), and Fe^{3+} (0.67 Å). With the increase of x/y concentrations the peaks associated with (200) reflection become wider, and a clear splitting for PFN_x-$PZT_{(1-x)}$ was seen for $x = 0.4$, while a narrow but asymmetrical peak was observed for the same composition for PFT_y-$PZT_{(1-y)}$. The temperature dependent XRD studies on PFT_y-$PZT_{(1-y)}$ for $y = 0.3$ and 0.4 showed an orthorhombic structure for these solid solutions at ambient temperature, but this is not obvious for smaller PFT concentrations y.

B. Raman spectroscopy

The room-temperature Raman spectra of PZT and PFN_x-$PZT_{(1-x)}$ ($x = 0.1$-0.4) are shown in Fig. 2. The Raman

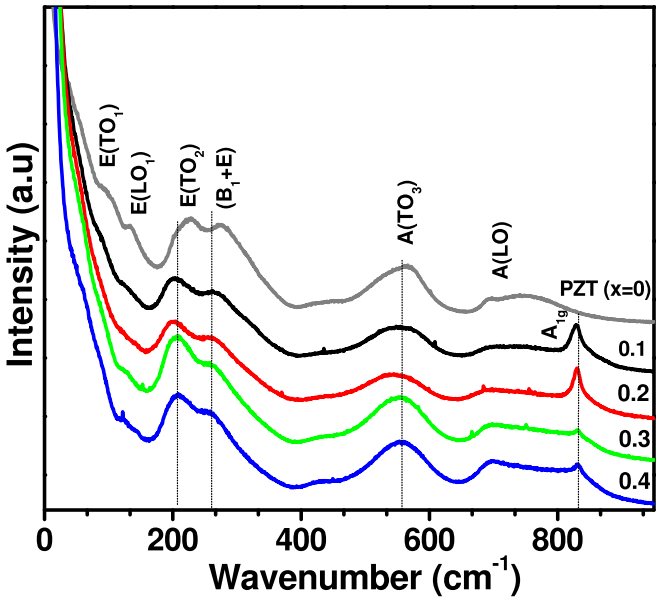

FIG. 2. Room temperature Raman spectra of PZT and $Pb(Fe_{0.5}Nb_{0.5})_x(Zr_{0.53}Ti_{0.47})_{(1-x)}O_3$ (x = 0.1, 0.2, 0.3, 0.4) ceramics.

spectrum of ceramic PZT contains a series of broad overlapping bands, which is typical of samples with tetragonal phase in this composition range.[31] According to the factor group analysis the tetragonal PZT has 12 optical normal modes of symmetry $\Gamma = 4E + 3A_1 + B_1$ that are Raman modes.[32] Raman spectra of PZT showed the low frequency phonon modes $E(TO_1)$ and $E(LO_1)$ at ~90 cm^{-1} and ~132 cm^{-1}; four additional peaks appeared at 224 cm^{-1}, 275 cm^{-1}, 565 cm^{-1}, and 740 cm^{-1}.[33] Raman spectra of PFN-PZT show a pseudo-tetragonal structure at room temperature for most concentration ranges, and so we assign these peaks to $E(TO_2)$, B_1+E and $A_1(TO_3)$, and $A_1(LO)$ modes, respectively.[33] Dilsom *et al.* reported for PFT-PZT (x = 0.3 and x = 0.4) that temperature dependent Raman and XRD studies revealed these materials are orthorhombic at room temperature. However, the lowest $E(TO_1)$ frequency mode is not seen clearly in PFN_x-$PZT_{(1-x)}$ spectrum because of strong Rayleigh scattering intensity. The modes $E(TO_2)$ and B_1+E correspond to BO_6 rotation, while $A_1(TO_3)$ and $A_1(LO)$ are related to O-B-O bending and B-O stretching of the oxygen octahedron, respectively.[34]

These modes shifted toward the lower frequencies with increase in the PFN contents. The decrease in wavenumber with increasing PFN contents is due to the difference in the atomic mass of Zr (91.22 g) and Ti (47.87 g) when they are replaced by Fe (55 g), and Nb (92.90 g) in the B site. The high frequency phonon mode at ~830 cm^{-1} appearing for x = 0.1-0.4 resembles to the A_{1g} phonon mode of PFN at 854 cm^{-1} which is attributed to the vibration of oxygen ions in the oxygen octahedra (Nb-O-Fe stretching mode).[35]

C. Electrical hysteresis loop (remanent polarization P_r and coercive field E_c)

The electric field induced polarization switching (*P-E*) behavior was studied at low frequency (50 Hz) utilizing Sawyer-Tower experimental set up. The electrical hysteresis loops for 10%, 20%, 30%, and 40% PFN are shown in Fig. 3(a), the strong ferroelectricity of PFN_x-$PZT_{(1-x)}$ was evidenced by well defined and saturated and low loss curves, with a remanent polarization of about 20-30 $\mu C\ cm^{-2}$. In general, enhancement in remanent polarization (P_r) and coercive field (E_c) were observed with increasing x, however an increase in the broadened the ferroelectric loop was seen with x, maybe due to increase in the conductivity. The evolution of P_r and E_c for PFN_x-$PZT_{(1-x)}$ and PFT_y-$PZT_{(1-y)}$ as a function of PFN-x and PFT-y concentrations, respectively, are shown in Figure 3(b). With increase of PFT-y concentration from y = 0.1 to 0.4 almost insignificant change in P_r (15–17 $\mu C\ cm^{-2}$), but E_c change from 10-15 kV cm^{-1}, while a significant increase in these quantities was observed with increase in PFN-x, i.e., P_r (17–31 μCcm^{-2}) and E_c (17-31 kV cm^{-1}). These values are comparable with other studies done in similar systems.[36–42]

D. Magnetic hysteresis (remanent magnetization M_r and coercive fields H_c)

Room temperature magnetization vs applied magnetic field curves of PFN_x-PZT_{1-x} ceramic are shown in

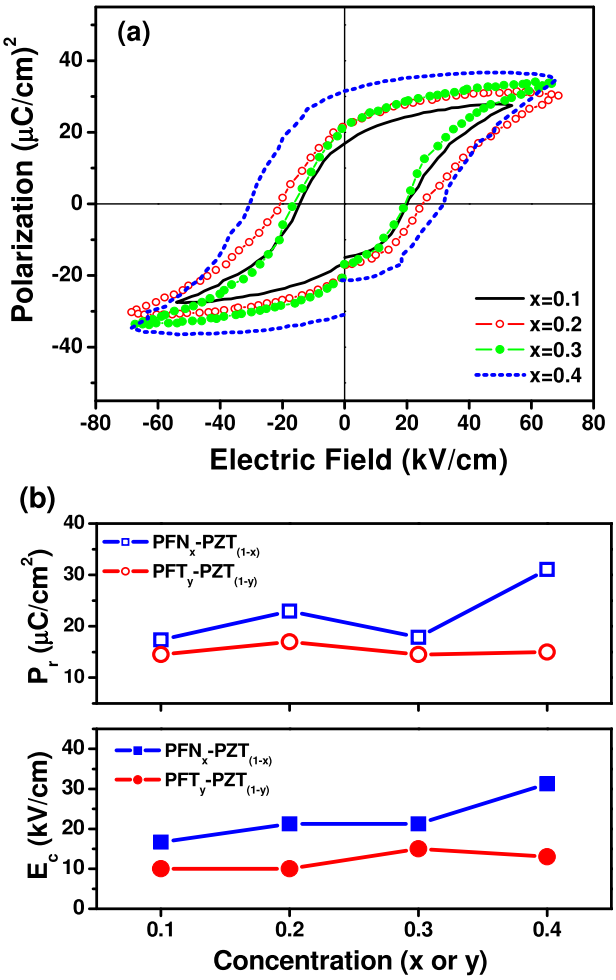

FIG. 3. Room temperature (a) Ferroelectric loop for $Pb(Fe_{0.5}Nb_{0.5})_x(Zr_{0.53}Ti_{0.47})_{(1-x)}O_3$ (x = 0.1, 0.2, 0.3, 0.4) ceramics. (b) Remanent polarization (P_r) and the respective electric coercive field (E_c) for PFN_x-$PZT_{(1-x)}$ and PFT_y-$PZT_{(1-y)}$ as a function of the concentration (x or y).

Fig. 4(a). Magnetization studies of these materials present well behaved magnetization (M) vs. applied magnetic field (H) loop at room temperature for PFN-x concentration between 0.1 and 0.4, however an improvement in magnetic properties was observed for $x = 0.2$ and $x = 0.3$, while a notable deterioration of the these properties was observed for $x = 0.4$. The remanent magnetization of PFN_x-PZT_{1-x} ($0.1 \leq x \leq 0.4$) has a maximum of ca. 0.06 emu g^{-1}, this is 7% of the maximum possible value for all Fe spins aligned at $T = 0$ and is gives some estimate of the degree of spin clustering at room temperature, the values obtained are comparables to the values reported by R. Blinc et al. for PFN ceramic multiferroic relaxor.[43] In Figure 4(b), we compare the remanent magnetization (M_r) and coercive magnetic field (H_c) obtained from M vs. H curve for PFN_x-PZT_{1-x} and PFT_y-PZT_{1-y} solid solution ceramic samples with x or y varying between 0.1 and 0.4. Similar trend for M_r and H_c was observed in both families, the higher magnetic properties were observed for $x/y = 0.2$.

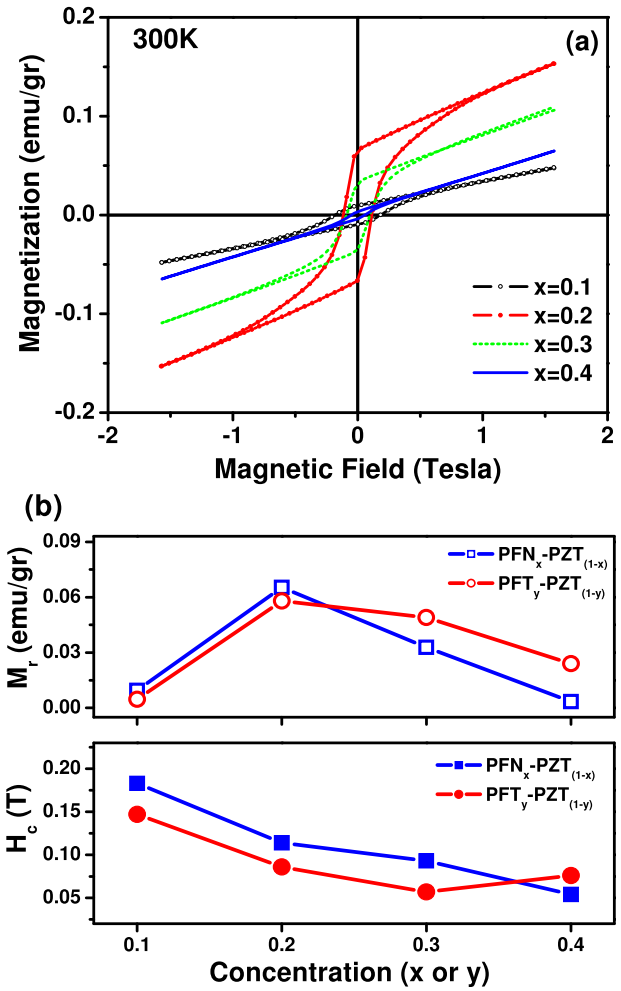

FIG. 4. Room temperature (a) ferromagnetic loop for $Pb(Fe_{0.5}Nb_{0.5})_x(Zr_{0.53}Ti_{0.47})_{(1-x)}O_3$ ($x = 0.1, 0.2, 0.3, 0.4$) ceramics. (b) Remanent magnetization (M_r) and the respective magnetic coercive field (H_c) for PFN_x-$PZT_{(1-x)}$ and PFT_y-$PZT_{(1-y)}$ as a function of the concentration (x or y).

E. Dielectric properties (capacitance, loss, and Curie temperatures)

The temperature variation of the dielectric constant (ε) and loss tangent ($\tan\delta$) for PFN_x-$PZT_{(1-x)}$ compositions were plotted in Fig. 5(a) at 10 kHz. It was not possible to measure the dielectric permittivity at higher temperature due to our experimental limitations in order to observe the phase transitions in sample with $x = 0.1$. However, we can see the variation of dielectric maximum temperature shifting toward lower temperature with increase in PFN composition. It is well known that the transition temperature (T_c) of PZT is $T_c \sim 690$ K,[40,44] with increase in x content of PFN_x-$PZT_{(1-x)}$ significant influence on the ferroelectric-paraelectric phase transition was observed. T_c decreased from ~689 K, to 585 K with x increasing from 0.2 to 0.4, respectively.

On the other hand, the temperature dependence of loss tangent for PFN_x-$PZT_{(1-x)}$ ceramics showed almost the same trend for all compositions with an increase of $\tan\delta$ with temperature, below 500 K. However, above 500 K, the composite samples showed a rapid increase with temperature depending upon the compositions. A noticeable increase in $\tan\delta$ accompanied by frequency dispersion is considered to be normal in ferroelectrics containing iron. The existence of the Fe ion, which is a transition element, may be responsible for the increased ionic conduction, resulting in the increase

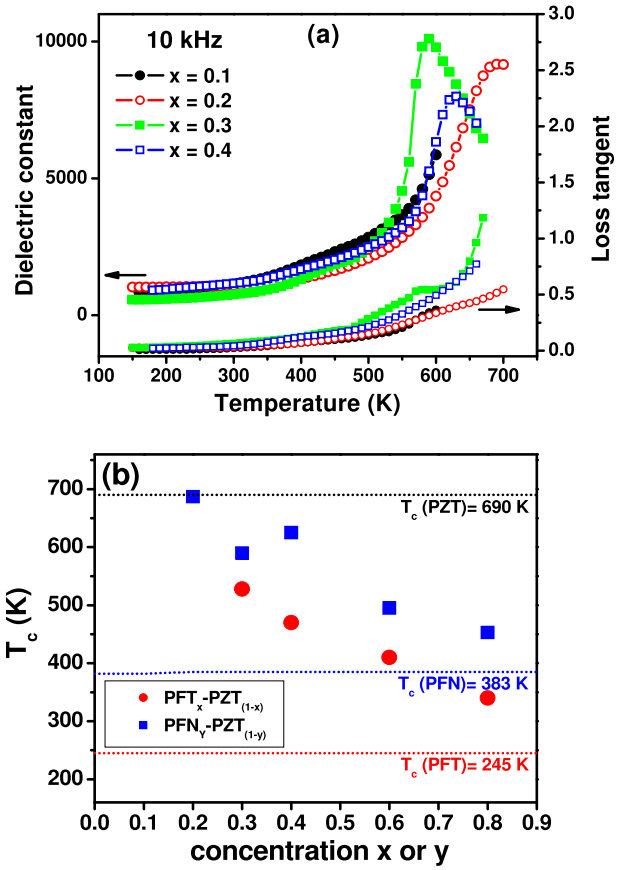

FIG. 5. (a) Temperature dependence of the dielectric constant PFN_x-$PZT_{(1-x)}$ ($x = 0.1, 0.2, 0.3, 0.4$) ceramics at 10 kHz. (b) Curie temperature (T_c) as a function of the x or y concentration for PFN_x-$PZT_{(1-x)}$ and PFT_y-$PZT_{(1-y)}$, respectively, dotted lines represent the T_c values of PZT, PFN, and PFT ceramic compounds.

in tanδ at higher temperatures. Figure 5(b) shows T_c as a function of x/y concentrations for PFN_x-$PZT_{(1-x)}$ and PFT_y-$PZT_{(1-y)}$, with increase in x/y contents, a significant influence on ferroelectric phase transition was observed. For PFN_x-$PZT_{(1-x)}$ the T_c value decreased from (687 K, x = 0.2) to (453 K, x = 0.8), while for PFT_y-$PZT_{(1-y)}$ the T_c shifted from higher temperature (~528 K, y = 0.3) to low temperature (~340 K, y = 0.8). The T_c values for PFN_x-$PZT_{(1-x)}$ and PFT_y-$PZT_{(1-y)}$ compounds are between ~690 K, T_c for PZT, x = 0 and 383 K, T_c for PFN, x = 1 or 245 K, T_c for PFT, y = 1 (Ref. 45), respectively, (see the horizontal lines in Fig. 5(b))

F. Transmission electron microscopy and field emission scanning electron microscopy (FESEM)

Field emission scanning electron microscope (FESEM) equipped with EDX by elemental composition mapping to the individual $Pb(Fe_{0.5}Nb_{0.5})_x(Zr_{0.53}Ti_{0.47})_{(1-x)}O_3$ (x = 0.2) grain of about 1 μm diameter (Fig. 6(a)) and $Pb(Fe_{0.5}Ta_{0.5})_y(Zr_{0.53}Ti_{0.47})_{(1-y)}O_3$ (y = 0.4) lamella cut by focus ion beam from the single grain (Fig. 6(b)). Figs. 6(a) and 6(b)-red square (upper) show the SEM image of the scanning area used to perform the compositional analysis for the respective material. Figure 6(a) (lower) show the elemental mapping results of the PFN_x-$PZT_{(1-x)}$ single grain that clearly reveal the presence of the all elements (Pb, Fe, Nb, Zr, Ti, and O) of the compound, it was evidenced the distribution of each element was highlighting homogeneous through of the grain. This experiment was done on several grains with similar results. Similar results were obtained for PFT_y-$PZT_{(1-y)}$ by mapping an area of about 700 nm × 400 nm in the lamella (see Figure 6(b)-lower).

G. Magnetoelectric coefficients

Preliminary measurements on bulk ceramic samples of the magnetoelectric coefficients $\alpha_{E,33}$ and $\alpha_{E,31}$ were carried out at 1 kHz and room temperature. The measurements were done for two field orientations: (i) in-plane mode for H and δH parallel to each other and to the sample plane and perpendicular to δE and (ii) out-of-plane mode for all the three fields (H, δH, and δE) parallel to each other and perpendicular to sample plane. Additional TEM studies done on the same samples in Belfast by Professor J. M. Gregg's group will be reported in a separate paper. For the 20% PFT/80% PZT specimen $\alpha_{E,31}$ was found (Figure 7) to be 12 mV (cm Oe)$^{-1}$. This is much smaller than the value for FIB single-crystals cut from our ceramic bulk samples;[50] the lower value presumably arises from averaging over domains and grains. The measurements of $\alpha_{E,33}$ (lower curve in Fig. 7) are symmetric with respect to change of sign in applied field +H

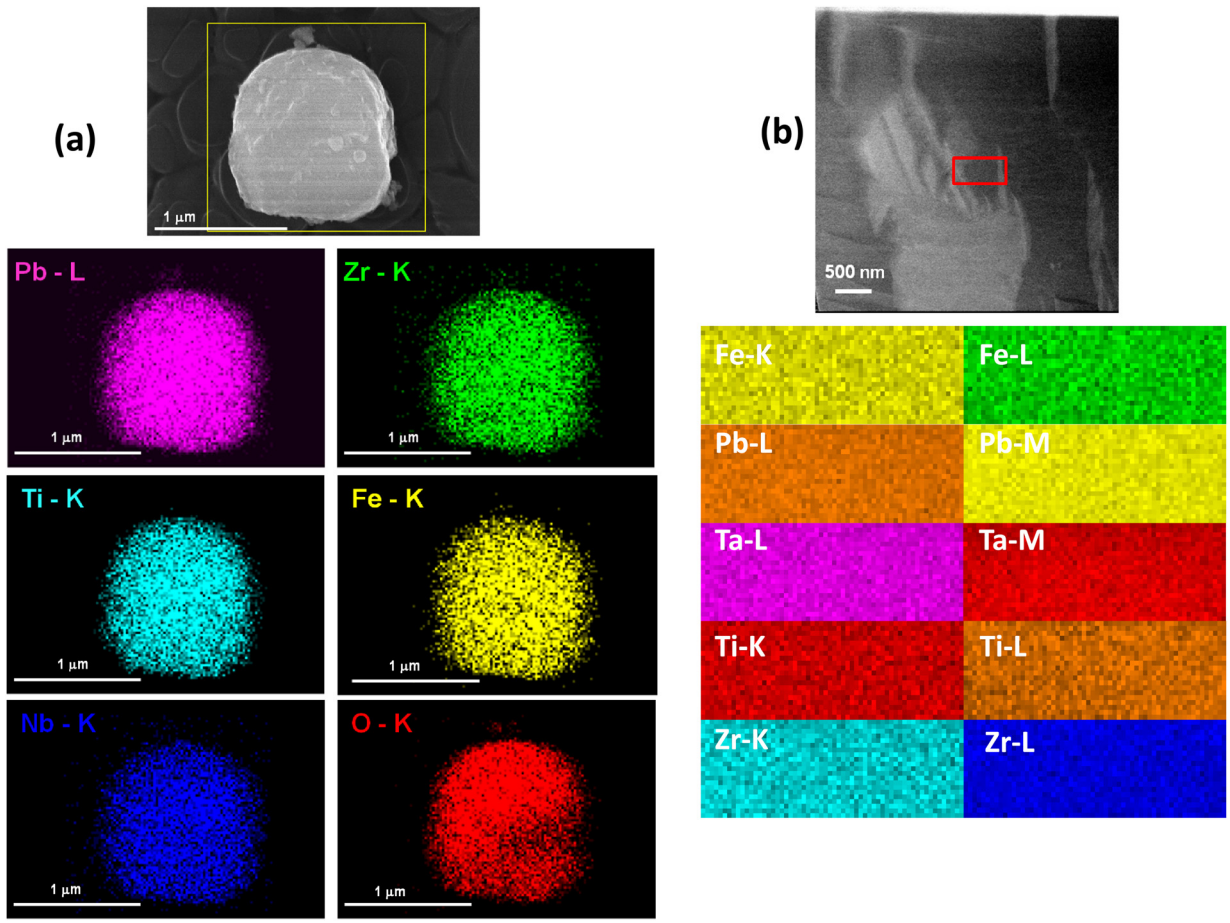

FIG. 6. SEM image (upper figure) for: (a) ~1 μm grain of $Pb(Fe_{0.5}Nb_{0.5})_x(Zr_{0.53}Ti_{0.47})_{(1-x)}O_3$ (x = 0.2) and (b) lamella of $Pb(Fe_{0.5}Ta_{0.5})_y(Zr_{0.53}Ti_{0.47})_{(1-y)}O_3$ (y = 0.4), ceramic samples. Lower figures in (a) and (b) represent the respective elemental concentration (Fe, Pb, Ti, Zr, Nb, Ta, and O) dot maps for each sample.

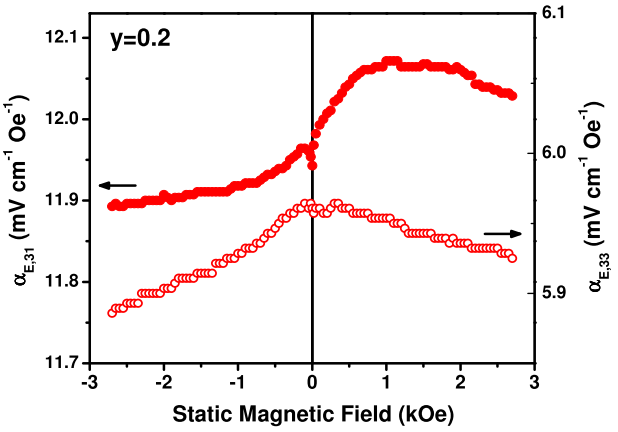

FIG. 7. ME voltage coefficient as a function of the bias magnetic field in longitudinal ($\alpha_{E,33}$) and transverse ($\alpha_{E,31}$) modes for PFT_y-$PZT_{(1-y)}$ ($y = 0.2$) at 1 kHz and room temperature.

or –H and therefore arise from a small biquadratic term P^2M^2 and not linear magnetoelectricity, which presumably averages to near zero values in this bulk specimen.

H. Theory

The PFT-PZT and PFN-PZT single-phase materials, we discuss here experimentally are not readily amenable to density functional theory (DFT) calculations for two reasons: First, the four B-site ions Zr, Ti, Fe, and Ta or Nb are not ordered, requiring very large unit cells in the simulations; second, the Fe spins are highly clustered, producing strong magnetoelectricity above the temperature at which long-range magnetic ordering occurs. In this respect these systems are probably good candidates for the Jahn-Teller model of Bersuker for magnetoelectrics,[46,47] which is based upon clusters, particularly for perovskite ferroelectrics such as those in the present work.

IV. CONCLUSIONS

In summary, we have successfully fabricate $(PbFe_{0.5}Nb_{0.5}O_3)_x(PbZr_{0.53}Ti_{0.47}O_3)_{(1-x)}$ and $(PbFe_{0.5}Ta_{0.5}O_3)_y(PbZr_{0.53}Ti_{0.47}O_3)_{(1-y)}$ ceramics by solid-state reaction route to produce single-phase room-temperature multiferroic magnetoelectrics. X- ray diffraction analysis and Raman spectra indicate that these PFN-PZT, PFT-PZT systems have perovskite crystal structure. The T_c values decrease from $T_{cPZT} \sim 690$ K toward $T_{cPFN} \sim 385$ K or $T_{cPFT} \sim 240$ K for PFN-PZT or PFT-PZT, respectively, however for all ceramic samples, in this study, the T_c value was above room temperature. Coexistence of biferroic nature i.e., ferroelectric and ferrogmatetic properties in PFN-PZT and PFT-PZT systems open the possibility to explore new family of materials which may exhibit the magnetoelectric effect at room temperature. These systems appear superior to bismuth ferrite for device applications in that their dielectric losses are much lower (ca. 1%).

Note added in proof. Evans *et al.*[50] measure 5.5×10^{-8} sm^{-1} to 1.3×10^{-7} sm^{-1} for α_{31} in 40:60 PFT/PZT at 293 K. These are very large values. We note also for completeness that PFN-PZT ceramic single-phase compounds were first studied in 1981 by Whatmore and Bell.[48,49]

ACKNOWLEDGMENTS

This work was supported in parts by DOE (DE-FG02-08ER46526), DOD (W911NF-11-1-0204) and NSF (EPS-1002410) grants. D. Sanchez was supported by an IFN-NSF Fellowship, while N. Ortega and A. Kumar were supported by DOE and DOD grants, respectively. The authors thank Frank Mendoza for his help with the FESEM-EDX measurements.

[1]A. Levstik, V. Bobnar, C. Filipič, J. Holc, M. Kosec, R. Blinc, Z. Trontel, and Z. Jagličić, Appl. Phys. Lett. **91**, 012905 (2007).
[2]D. A. Sanchez, A. Kumar, N. Ortega, R. S. Katiyar, and J. F. Scott, Appl. Phys. Lett. **97**, 202910 (2010).
[3]R. Blinc, V. Laguta, B. Zalar, B. Zupančič, and M. Itoh, J. Appl. Phys. **104**, 084105 (2008).
[4]W. Peng, N. Lemee, J. Holc, M. Kosec, R. Blinc, and M. G. Karkut, J. Magn. Magn. Mater. **321**, 1754 (2009).
[5]W. Peng, N. Lemee, M. Karkut, B. Dkhil, V. V. Shvartsman, P. Borisov, W. Kleemann, J. Holc, M. Kosec, and R. Blinc, Appl. Phys. Lett. **94**, 012509 (2009).
[6]M. Correa, A. Kumar, S. Priya, R. S. Katiyar, and J. F. Scott, Phys. Rev. B **83**, 014302 (2011).
[7]A. Kumar, R. S. Katiyar, and J. F. Scott, IEEE Trans. Ultrason., Ferroelectr., Freq. Control **57**, 2237 (2010).
[8]D. Sanchez, N. Ortega, R. S. Katiyar *et al.*, in Conference: 2012 Joint 21st IEEE ISAF/11th IEEE ECAPD/IEEE PFM (ISAF/ECAPD/PFM), Aveiro, Portugal, 9-13 July 2012.
[9]A. Kumar, R. S. Katiyar, and J. F. Scott, J. Appl. Phys. **108**, 064105 (2010).
[10]A. Kumar, G. L. Sharma, R. S. Katiyar, and J. F. Scott, J. Phys.: Condens. Matter **21**, 382204 (2009).
[11]A. Kumar, R. S. Katiyar, and J. F. Scott, Appl. Phys. Lett. **94**, 212903 (2009).
[12]A. Kumar, I. Rivera, R. S. Katiyar, and J. F. Scott, Appl. Phys. Lett. **92**, 132913 (2008).
[13]A. Kumar, N. M. Murari, R. S. Katiyar, and J. F. Scott, Appl. Phys. Lett. **90**, 262907 (2007).
[14]A. Kumar, R. S. Katiyar, R. N. Premnath, C. Rinaldi, and J. F. Scott, J. Mater. Sci. **44**, 5113 (2009).
[15]J. F. Scott, "Applications of modern ferroelectrics," Science **315**, 954 (2007).
[16]D. A. Sánchez, N. Ortega, A. Kumar, R. Roque-Malherbe, R. Polanco, J. F. Scott, and R. S. Katiyar, AIP Adv. **1**, 042169 (2011).
[17]A. Kumar, J. F. Scott, and R. S. Katiyar, Appl. Phys. Lett. **99**, 042907 (2011).
[18]M. Gajek, M. Bibes, S. Fusil, K. Bouzehouane, J. Fontcuberta, A. Barthélémy, and A. Fert, Nature Mater. **6**, 296 (2007).
[19]J. F. Scott, Nature Mater. **6**, 256 (2007).
[20]J. F. Scott, ChemPhysChem **10**, 1761 (2009).
[21]H. Béa, M. Gajek, M. Bibes, and A. Barthélémy, J. Phys.: Condens. Matter **20**, 434221 (2008).
[22]C. Israel, N. D. Mathur, and J. F. Scott, Nature Mater. **7**, 93 (2008).
[23]V. García, S. Fusil, K. Bouzehouane, S. Enouz-Vedrenne, N. D. Mathur, A. Barthélémy, and M. Bibes, Nature **460**, 81 (2009).
[24]Y.-H. Chu, L. W. Martin, M. B. Holcomb, M. Gajek, S.-J. Han, Q. He, N. Balke, Ch.-H. Yang, D. Lee, W. Hu, Q. Zhan, P.-L. Yang, A. Fraile-Rodríguez, A. Scholl, Sh. X. Wang, and R. Ramesh, Nature Mater. **7**, 478 (2008).
[25]V. García, M. Bibes, L. Bocher S. Valencia, F. Kronast, A. Crassous, X. Moya, S. Enouz-Vedrenne, A. Gloter, D. Imhoff, C. Deranlot, N. D. Mathur, S. Fusil, K. Bouzehouane, and A. Barthélémy, Science **327**, 1106 (2010).
[26]K. Takahashi, N. Kida, and M. Tonouchi, Phys. Rev. Lett. **96**, 117402 (2006).
[27]J. F. Scott, H. J. Fan, S. Kawasaki, J. Banys, M. Ivanov, A. Krotkus, J. Macutkevic, R. Blinc, V. V. Laguta, P. Cevc, J. S. Liu, and A. L. Kholkin, Nano Lett. **8**, 4404 (2008).

[28]G. Catalan and J. F. Scott, Adv. Mater. **21**, 2463 (2009).
[29]R. Pirc, R. Blinc, and J. F. Scott, Phys. Rev. B **79**, 214114 (2009).
[30]S. Kamba, in Nature-sponsored conference on oxides, Aachen, Germany, July 2012.
[31]S. Takahashi, S. Hirose, and K. Uchino, J. Am. Ceram. Soc. **77**, 2429 (1994).
[32]J. Frantti, V. Lantto, and J. Lappalainen, J. Appl. Phys. **79**, 1065 (1996).
[33]J. F. Meng, R. S. Katiyar, G. T. Zou, and X. H. Wang, Phys. Status Solidi A **164**, 851 (1997).
[34]M. K. Zhu, P. X. Lu, Y. D. Hou, X. M. Song, H. Wang, and H. Yan, J. Am. Ceram. Soc. **89**, 3739 (2006)
[35]A. F. Garcia Flores, D. A. Tenne, Y. J. Choi, W. J. Ren, X. X. Xi, and S. W. Cheong, J. Phys.: Condens. Matter **23**, 015401 (2011).
[36]N. Kumar, A. Ghosh, and R. N. P. Choudhary, Mater. Chem. Phys. **130**, 381 (2011).
[37]B.-J. Fang, C.-L. Ding, W. Liu, L.-Q. Li and L. Tang, Eur. Phys. J. Appl. Phys. **45**, 20302 (2009).
[38]M. Yokosuka, "Electrical, electromechanical and structural studies on solid solution ceramic $Pb(Fe_{1/2}Nb_{1/2})O_3$–$Pb(Zn_{1/3}Nb_{2/3})O_3$," Jpn. J. Appl. Phys., Part 1 **38**, 5488 (1999).
[39]J. S. Kim, J. H. Jeong, S. Y. Cho, M. S. Jang, and S.-B. Cho, J. Korean Phys. Soc. **51**, S133 (2007).
[40]C. A. Randall, N. Kim, J. P. Kucera, W. Cao, and T. R. Shrout, J. Am. Ceram. Soc. **81**, 677 (1998).
[41]R. Font, O. Raymond, E. Martinez, J. Portelles, and J. M. Siqueiros, J. Appl. Phys. **105**, 114110 (2009).
[42]S. Nomura, H. Takabayashi, and T. Nakagawa, Jpn. J. Appl. Phys., Part 1 **7**, 600 (1968).
[43]R. Blinc, P. Cevc, A. Zorko, J. Holc, M. Kosec, Z. Trontelj, J. Pirnat, N. Dalal, V. Ramachandran, and J. Krzystek, J. Appl. Phys. **101**, 033901 (2007).
[44]P. Jaita, A. Watcharapasorn, and S. Jiansirisomboon, Solid State Sci. **12**, 1608 (2010).
[45]B. H. Lee, N. K. Kim, J. J. Kim, and S. H. Cho, J. Korean Phys. Soc. **32**, S978 (1998).
[46]I. B. Bersuker, Adv. Quantum Chem. **44**, 1 (2003).
[47]P. Garcia-Fernandez and I. B. Bersuker, Phys. Rev. Lett. **106**, 246406 (2011).
[48]R. W. Whatmore and A. J. Bell, Ferroelectrics **35**, 155 (1981).
[49]A. J. Bell and W. Whatmore, Ferroelectrics **37**, 543 (1981).
[50]D. M. Evans, A. Schilling, Ashok Kumar, D. Sanchez, N. Ortega, M. Arredondo, R. S. Katiyar, J. M. Gregg, and J. F. Scott, "Magnetic Switching of Ferroelectric Domains at Room Temperature in a New Multiferroic," Nat. Commun. (in press).